XIV International Conference on Computational Plasticity. Fundamentals and Applications
COMPLAS XIV
E. Oñate, D.R.J. Owen, D. Peric & M. Chiumenti (Eds)

MATLAB PARALLEL CODES FOR 3D SLOPE STABILITY BENCHMARKS

MARTIN CERMAK* AND VACLAV HAPLA* AND DAVID HORAK*†

* VSB-TU Ostrava
IT4Innovations National Supercomputing Center (IT4I)
Studentska 6231/1b, 708 00 Ostrava, Czech Republic
email: martin.cermak@vsb.cz - web page: http://www.it4i.cz

† VSB-TU Ostrava
Department of Applied Mathematics
17. listopadu 15/2172, 708 00 Ostrava, Czech Republic

Key words: Computational Plasticity, TFETI, MATLAB, Parallel implementation, Mohr-Coulomb

Abstract. This contribution is focused on a description of implementation details for solver related to the slope stability benchmarks in 3D. Such problems are formulated by the standard elastoplastic models containing the Mohr-Coulomb yield criterion and by the limit analysis of collapse states. The implicit Euler method and higher order finite elements are used for discretization. The discretized problem is solved by non-smooth Newton-like methods in combination with incremental methods of limit load analysis.

In this standard approach, we propose several innovative techniques. Firstly, we use recently developed sub-differential based constitutive solution schemes. Such an approach is suitable for non-smooth yield criteria, and leads better return-mapping algorithms. For example, a priori decision criteria for each return-type or simplified construction of consistent tangent operators are applied.

The parallel codes are developed in MATLAB using Parallel Computing Toolbox. For parallel implementation of linear systems, we use the TFETI domain decomposition method. It is a non-overlapping method where the Lagrange multipliers are used to enforce continuity on the subdomain interfaces and satisfaction of the Dirichlet boundary conditions.

1 INTRODUCTION

In our paper, we focus on parallel implementation of the new approach introduced in [12], which is based on MATLAB codes. The parallelization is based on the TFETI domain decomposition method [5], which is a modification of the original FETI method proposed by Farhat and Roux [7].

We investigated the parallel implementation of a solver for small-strain, quasi-static elastoplastic problem that contains the Mohr-Coulomb yield criterion, associative flow rule, and perfect plasticity. The incremental constitutive problem is usually solved by the elastic predictor/plastic corrector method. The plastic correction is also called (implicit) return-mapping scheme. The improved scheme in [12] is based on the sub-differential formulation of the plastic flow rule. It leads to a priori information whether the unknown stress tensor lies on the smooth portion, on the "left" edge, on the "right" edge, or at the apex of the pyramidal yield surface, even if the nonlinear isotropic hardening is considered within the model.

The procedure of solving the problem in parallel is very similar to the classical solution. The main differences are: a) the original mesh is partitioned by METIS [10] into subdomains, and it is necessary to assemble the TFETI objects for each subdomain such as the equality constraint matrix and the kernel matrix, and these matrices do not change during the computation process [13]; b) the stiffness matrix, right hand side and other objects are assembled for each subdomain in each Newton step; c) in each Newton step, the dual formulation in the Lagrange multipliers is solved instead of the primal formulation in displacement; d) in contrast to the approach introduced in [12] where two loops (loading step, Newton step) are considered, we add another loop for the iterative solver (conjugate gradient) which solved the linearized problem in each Newton iteration.

In the text, we assume a deformable body from an elastoplastic material. The material model contains the Mohr-Coulomb yield criterion, the associative flow rule, and the nonlinear hardening law as in [2, 4]. For the sake of simplicity, consider an elasto-plastic problem in 3D. Let Ω be a polygonal 3D domain and $\mathcal{T}_h$ denote its triangulation. Further, consider linear and conforming elements. So the displacement fields are approximated by continuous and piecewise linear functions, and the strain, stress and isotropic hardening fields are approximated by piecewise constant functions.

The paper is organized as follows. In Section 2, we introduce the initial value constitutive problem for the Mohr-Coulomb plastic criterion with the implicit Euler time discretization; in Section 3, we summarize the TFETI domain decomposition method and algebraic formulation of our investigated problem; in Section 4, several implementation details for the parallel code in MATLAB are briefly summarized. We illustrate the performance of our algorithm on the slope stability benchmark in 3D in Section 5.

2 THE CONSTITUTIVE INITIAL VALUE PROBLEM OF THE MOHR-COULOMB CRITERION AND THE IMPLICIT EULER DISCRETIZATION

The initial value constitutive problem reads:

Given the history of the strain tensor $\boldsymbol{\varepsilon} = \boldsymbol{\varepsilon}(t)$, $t \in [0, t_{\max}]$, *and the initial values* $\boldsymbol{\varepsilon}^p(0) = \boldsymbol{\varepsilon}^p_0$, $\bar{\varepsilon}^p(0) = \bar{\varepsilon}^p_0$, *find* $(\boldsymbol{\sigma}(t), \boldsymbol{\varepsilon}^p(t), \bar{\varepsilon}^p(t))$ *such that the conditions*

$$\left.\begin{aligned} \boldsymbol{\sigma} = \mathbb{D}_e : (\boldsymbol{\varepsilon} - \boldsymbol{\varepsilon}^p), \quad \kappa = H(\bar{\varepsilon}^p), \\ \dot{\boldsymbol{\varepsilon}^p} \in \dot{\lambda} \partial g(\boldsymbol{\sigma}), \quad \dot{\bar{\varepsilon}}^p = -\dot{\lambda} \tfrac{\partial f(\boldsymbol{\sigma}, \kappa)}{\partial \kappa}, \\ \dot{\lambda} \geq 0, \quad f(\boldsymbol{\sigma}, \kappa) \leq 0, \quad \dot{\lambda} f(\boldsymbol{\sigma}, \kappa) = 0. \end{aligned}\right\} \tag{1}$$

hold for each instant $t \in [0, t_{\max}]$.

Here, $\boldsymbol{\sigma}, \boldsymbol{\varepsilon}^p, \bar{\varepsilon}^p, \lambda$ denote the Cauchy stress tensor, the plastic strain, the hardening variable, and the plastic multiplier, respectively. The dot symbol means the pseudo-time derivative of a quantity. The functions f and g represent the yield function and the plastic potential for the Mohr-Coulomb model, respectively. They are defined as:

$$f(\boldsymbol{\sigma}, \kappa) = (1 + \sin\phi)\omega_1(\boldsymbol{\sigma}) - (1 - \sin\phi)\omega_3(\boldsymbol{\sigma}) - 2(c_0 + \kappa)\cos\phi, \tag{2}$$

$$g(\boldsymbol{\sigma}) = (1 + \sin\psi)\omega_1(\boldsymbol{\sigma}) - (1 - \sin\psi)\omega_3(\boldsymbol{\sigma}), \tag{3}$$

where ω_1 and ω_3 are the maximal and minimal eigenvalue functions, and $\partial f(\boldsymbol{\sigma}, \kappa)/\partial\kappa = -2\cos\phi$.

Further, the fourth order tensor $\mathbb{D}_e$ represents the linear isotropic elastic law

$$\boldsymbol{\sigma} = \mathbb{D}_e : \boldsymbol{\varepsilon}^e = \frac{1}{3}(3K - 2G)(\boldsymbol{I} : \boldsymbol{\varepsilon}^e)\boldsymbol{I} + 2G\boldsymbol{\varepsilon}^e, \quad \mathbb{D}_e = \frac{1}{3}(3K - 2G)\boldsymbol{I} \otimes \boldsymbol{I} + 2G\mathbb{I}, \tag{4}$$

where $\boldsymbol{\varepsilon}^e = \boldsymbol{\varepsilon} - \boldsymbol{\varepsilon}^p$, K and G $(K, G > 0)$ denote the elastic part of the strain tensor, bulk and shear moduli, respectively.

Finally, we let the function H representing the non-linear isotropic hardening in an abstract form and assume that it is a nondecreasing, continuous, and piecewise smooth function satisfying $H(0) = 0$.

It is worth mentioning that the value t_{max} need not be always known. Let

$$0 = t_0 < t_1 < \ldots < t_k < \ldots < t_N = t_{\max}$$

be a partition of the interval $[0, t_{\max}]$ and denote $\boldsymbol{\sigma}_k := \boldsymbol{\sigma}(t_k)$, $\boldsymbol{\varepsilon}_k := \boldsymbol{\varepsilon}(t_k)$, $\boldsymbol{\varepsilon}^p_k := \boldsymbol{\varepsilon}^p(t_k)$, $\bar{\varepsilon}^p_k := \bar{\varepsilon}^p(t_k)$, $\bar{\varepsilon}^{p,tr}_k := \bar{\varepsilon}^p(t_{k-1})$, $\boldsymbol{\varepsilon}^{tr}_k := \boldsymbol{\varepsilon}(t_k) - \boldsymbol{\varepsilon}^p(t_{k-1})$, and $\boldsymbol{\sigma}^{tr}_k := \mathbb{D}_e : \boldsymbol{\varepsilon}^{tr}_k$. Here, the superscript tr denotes the so-called trial variables (see, e.g., [4]) which are known. If it is clear that the step k is fixed, then we will omit the subscript k and write $\boldsymbol{\sigma}$, $\boldsymbol{\varepsilon}$, $\boldsymbol{\varepsilon}^p$, $\bar{\varepsilon}^p$, $\bar{\varepsilon}^{p,tr}$, $\boldsymbol{\varepsilon}^{tr}$, and $\boldsymbol{\sigma}^{tr}$ to simplify the notation. The k-th step of the incremental constitutive problem discretized by the implicit Euler method reads:

Given $\boldsymbol{\sigma}^{tr}$ *and* $\bar{\varepsilon}^{p,tr}$*, find* $\boldsymbol{\sigma}$*,* $\bar{\varepsilon}^p$*, and* $\triangle\lambda$ *satisfying*

$$\left.\begin{aligned} \boldsymbol{\sigma} = \boldsymbol{\sigma}^{tr} - \triangle\lambda\mathbb{D}_e : \boldsymbol{\nu}, \quad \boldsymbol{\nu} \in \partial g(\boldsymbol{\sigma}), \\ \bar{\varepsilon}^p = \bar{\varepsilon}^{p,tr} + \triangle\lambda(2\cos\phi), \\ \triangle\lambda \geq 0, \quad f(\boldsymbol{\sigma}, H(\bar{\varepsilon}^p)) \leq 0, \quad \triangle\lambda f(\boldsymbol{\sigma}, H(\bar{\varepsilon}^p)) = 0. \end{aligned}\right\} \tag{5}$$

Unlike Problem (1), the unknown $\boldsymbol{\varepsilon}^p$ is not introduced in (5). It can be simply computed from the formula $\boldsymbol{\varepsilon}^p(t_k) = \boldsymbol{\varepsilon}(t_k) - \mathbb{D}_e^{-1} : \boldsymbol{\sigma}(t_k)$ and used as the input parameter for the next step. To solve the incremental problem, we use the standard elastic predictor/plastic corrector method.

The elastic predictor. First, we verify whether the trial generalized stress $(\boldsymbol{\sigma}^{tr}, \bar{\varepsilon}^{p,tr})$ is admissible:

$$f(\boldsymbol{\sigma}^{tr}, H(\bar{\varepsilon}^{p,tr})) \leq 0. \tag{6}$$

If this inequality holds, then we set

$$\boldsymbol{\sigma} = \boldsymbol{\sigma}^{tr}, \quad \bar{\varepsilon}^p = \bar{\varepsilon}^{p,tr}, \quad \triangle\lambda = 0.$$

It is readily seen that the triplet $(\boldsymbol{\sigma}, \bar{\varepsilon}^p, \triangle\lambda)$ solves the incremental problem.

The plastic corrector (the implicit return-mapping scheme). Let (6) not hold and assume that the incremental constitutive problem has a solution. Then clearly $\triangle\lambda > 0$, and the problem reduces into the following form:
Given $\boldsymbol{\varepsilon}^{e,tr}$ and $\bar{\varepsilon}^{p,tr}$ such that $f(\boldsymbol{\sigma}^{tr}, H(\bar{\varepsilon}^{p,tr})) > 0$, find $\boldsymbol{\sigma}$, $\bar{\varepsilon}^p$ and $\triangle\lambda > 0$ satisfying

$$\left.\begin{aligned} \boldsymbol{\sigma} = \boldsymbol{\sigma}^{tr} - \triangle\lambda\mathbb{D}_e : \boldsymbol{\nu}, \quad \boldsymbol{\nu} \in \partial g(\boldsymbol{\sigma}), \\ \bar{\varepsilon}^p = \bar{\varepsilon}^{p,tr} + \triangle\lambda(2\cos\phi), \\ f(\boldsymbol{\sigma}, H(\bar{\varepsilon}^p)) = 0. \end{aligned}\right\} \tag{7}$$

If the plastic potential g is differentiable on the yield surface, then the flow direction $\boldsymbol{\nu}$ is always single valued, and the return-mapping scheme leads to solving a system of nonlinear equations. In [12] you can find details how to return to the smooth portion, to the "left" edge, to the "right" edge, and to the apex of the pyramidal yield surface, as well as how to construct nonlinear and tangential operators. The algebraic formulation of the elastoplastic problem is formulated in [3] for the Drucker-Prager criterion and in [14] for the von Mises criterion in combination with TFETI, which is summarized in the following section.

As we mentioned above, we solved the nonlinear system of equations in each time step. The semi-smooth Newton method [11] is applied to the nonlinear system of equations in order to linearize it.

After preparing the tangential stiffness matrix and load vectors according to [12], we can formulate the following problem:
Find increment of displacement $\triangle\boldsymbol{u}_{k+1} \in \boldsymbol{V}$ so that

$$\boldsymbol{v}^T \left(\boldsymbol{F}_k(\triangle\boldsymbol{u}_{k+1}) - \triangle\boldsymbol{f}_{k+1}\right) = 0 \quad \forall \boldsymbol{v} \in \boldsymbol{V}, \tag{8}$$

where $\triangle\boldsymbol{f}_{k+1}$ is the increment of the load vector, $\boldsymbol{F}_k$ is the nonlinear operator, and $\boldsymbol{V}$ is the set of admissible displacements

$$\boldsymbol{V} = \{\boldsymbol{v} \in \mathbb{R}^n | \boldsymbol{B}_U\boldsymbol{v} = \boldsymbol{o}\}.$$

The relation $\boldsymbol{B}_U\boldsymbol{v} = \boldsymbol{o}$ represents the Dirichlet boundary conditions. The nonlinear equations (8) can be linearized by the semi-smooth Newton method.

3 TFETI AND ALGEBRAIC FORMULATION OF THE PROBLEM FOR ELASTO-PLASTIC BODIES

To apply the Total FETI (TFETI) domain decomposition method (DDM), we tear the body from the part of the boundary with the Dirichlet boundary condition, decompose it into subdomains, assign each subdomain a unique number, and introduce new "gluing"

conditions on the artificial subdomain interfaces and on the boundaries with the imposed Dirichlet condition. Let s denote the total number of the subdomains.

In the case of TFETI, the global stiffness matrix $\mathbf{K}$ and right-hand side $\mathbf{f}$ are assembled only subdomain-wise, and take the form

$$\mathbf{K} = \mathrm{diag}(\mathbf{K}^1, \ldots, \mathbf{K}^s),$$
$$\mathbf{f} = [(\mathbf{f}^1)^T, \ldots, (\mathbf{f}^s)^T]^T,$$

where $\mathbf{K}^p$ and $\mathbf{f}^p$, $p = 1, \ldots, s$, are the fully assembled stiffness matrix and load vector of the subdomain Ω^p, respectively. Then also the unknown vector of displacements $\mathbf{u}$ can be subdivided as

$$\mathbf{u} = [(\mathbf{u}^1)^T, \ldots, (\mathbf{u}^s)^T]^T,$$

where $\mathbf{u}^p$, $p = 1, \ldots, s$, is the vector of displacements of subdomain Ω^p.

TFETI is a dual approach, which means that the interface compatibility is enforced by introducing the Lagrange multipliers. In the case of TFETI, also the Dirichlet boundary conditions are enforced (see Figure 1) in this way whereas $\mathbf{K}^p$ remains unchanged, and hence it is singular. The resulting equality constraints can be written as

$$\mathbf{B}\mathbf{u} = \mathbf{o},$$

where $\mathbf{B}$ is a signed Boolean matrix. It can be split vertically into two blocks corresponding to the gluing part $\mathbf{B}_G$ and the Dirichlet part $\mathbf{B}_D$.

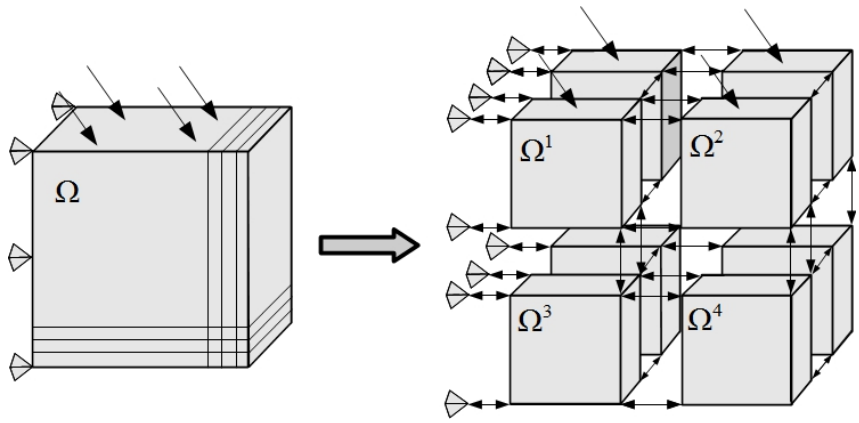

Figure 1: The TFETI domain decomposition method for unit cube.

Introducing the Lagrange multipliers $\boldsymbol{\lambda}$ to enforce the interface compatibility, the global problem takes the equivalent primal-dual form

$$\begin{bmatrix} \mathbf{K} & \mathbf{B}^T \\ \mathbf{B} & \mathbf{O} \end{bmatrix} \begin{bmatrix} \mathbf{u} \\ \boldsymbol{\lambda} \end{bmatrix} = \begin{bmatrix} \mathbf{f} \\ \mathbf{o} \end{bmatrix}. \tag{9}$$

Let us establish notation

$$\mathbf{F} = \mathbf{B}\mathbf{K}^{\dagger}\mathbf{B}^{T}, \quad \mathbf{G} = -\mathbf{R}^{T}\mathbf{B}^{T}, \quad \mathbf{d} = \mathbf{B}\mathbf{K}^{\dagger}\mathbf{f}, \quad \mathbf{e} = -\mathbf{R}^{T}\mathbf{f}.$$

$\mathbf{K}^{\dagger}$ denotes a generalized inverse of $\mathbf{K}$, satisfying $\mathbf{K}\mathbf{K}^{\dagger}\mathbf{K} = \mathbf{K}$. Notice $\mathbf{K}^{\dagger}$ inherits the block-diagonal structure from $\mathbf{K}$ and each block $(\mathbf{K}^{\dagger})^{p}$ is the generalized inverse of $\mathbf{K}^{p}$. We obtain a new linear system with unknowns $\boldsymbol{\lambda}$ and $\boldsymbol{\alpha}$

$$\begin{bmatrix} \mathbf{F} & \mathbf{G}^{T} \\ \mathbf{G} & \mathbf{O} \end{bmatrix} \begin{bmatrix} \boldsymbol{\lambda} \\ \boldsymbol{\alpha} \end{bmatrix} = \begin{bmatrix} \mathbf{d} \\ \mathbf{e} \end{bmatrix}. \tag{10}$$

For more details about solving this system and preconditioning, see [6, 1].

4 IMPLEMENTATION DETAILS

Our parallel implementation is based on the TFETI DDM. To apply this method, the original domain is partitioned into subdomains first. One of the widely used software tools for this task is METIS [10], which allows meshes to be partitioned in 2D and 3D. This software returns the number of subdomains for each element in the original mesh. Based on this partitioning, we assemble the objects for each individual subdomains independently. The local-to-global maping is constructed and the elements and nodes belonging to the interface are identified in order to assemble the equality constraint matrix B.

The equality constraint matrix $\mathbf{B}$ consists of the Dirichlet part $\mathbf{B}_D$ and the gluing part $\mathbf{B}_G$. We have three ways how to assemble the gluing part $\mathbf{B}_G$: redundant, non-redundant and orthonormal case, see [8]. In our code we allow all options but we recommend a) and c) for better convergence.

Two well known preconditioners were implemented: Dirichlet and lumped, see [6, 1]. The Dirichlet preconditioner needs a smaller number of CG iterations but is more expensive than the lumped one.

In our implementation, we use three loops: the outer loop for the loading process represents the direct method; the middle loop for the semi-smooth Newton method; and the inner loop for the linear iteration solver, more specifically the preconditioned conjugate gradient method with projector (PCGP). The first two loops were introduced in [12] in detail and the last one in [14].

For parallel computation, we use MATLAB Distributed Computing Server and MATLAB Parallel Toolbox for sending and receiving data via its Message Passing Interface (MPI) wrappers.

5 NUMERICAL EXPERIMENTS

We implemented the direct method of incremental limit analysis in MATLAB for the 3D slope stability problem. The code is parallelized by MATLAB Parallel Toolbox as we mentioned in the previous section, and includes the improved return-mapping scheme for the Mohr-Coulomb model. The available options include a) several types of finite elements with appropriate numerical quadratures; b) locally refined meshes with various densities; c) different preconditioners; d) different types of the equality constraint matrix.

We consider the extension of the benchmark for the plane strain problem introduced in [4, Page 351] for the 3D case. Further, we set $E = 20\,000\,\text{kPa}$, $\nu = 0.49$, $\phi = 20°$ and $c = 50\,\text{kPa}$, where c denotes the cohesion for the perfect plastic model. The stopping tolerance of the Newton and CG loops are set to $\epsilon_{Newton} = 10^{-7}$ and $\epsilon_{CG} = 10^{-12}$, respectively.

All numerical experiments were computed on the Salomon supercomputer. The Salomon cluster consists of 1008 compute nodes, totaling 24,192 compute cores with 129 TB RAM and giving over 2 Pflop/s theoretical peak performance. Each node is a powerful x86-64 computer, equipped with 24 cores, at least 128 GB RAM. The nodes are interconnected by 7D Enhanced hypercube InfiniBand network and equipped with the Intel Xeon E5-2680v3 processors. The Salomon cluster consists of 576 nodes without accelerators and 432 nodes equipped with the Intel Xeon Phi MIC accelerators.

Within this slope stability experiment, we compared the loading paths for the Q1 and Q2 hexahedral elements with 8 and 20 nodes, respectively, simillarly as in [12]. We consider $2 \times 2 \times 2$ and $3 \times 3 \times 3$ nodes integration quadratures for these element types, respectively. For the Q1 elements, the meshes contain 5103 and 37597 nodal points. For the Q2 elements, the meshes contain 19,581 and 147,257 nodal points. We use the direct method of the incremental limit analysis which is terminated when the computed settlement exceeds 4 meters. For parallel computing, we use 4 and 20 cores on Salomon for level 1 and 2, respectively.

The corresponding loading paths are depicted in Figure 2. We can see that the loading paths are very similar to loading paths which were introduced in [12]. Figure 3 illustrates a failure at the end of the loading process for the Q2 elements and the finer mesh.

The computation time of our approach is worse than the time which we need for the sequential version of the code in MATLAB, but this implementation gives us the opportunity to compute bigger problems and guidelines how to implement it more efficiently for example in our PERMON toolbox [9].

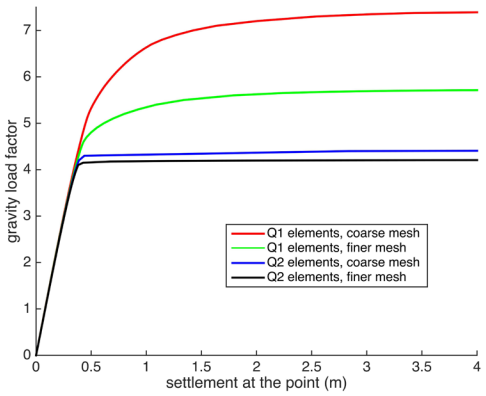

Figure 2: Comparison of the loading paths for $Q1$ and $Q2$ elements.

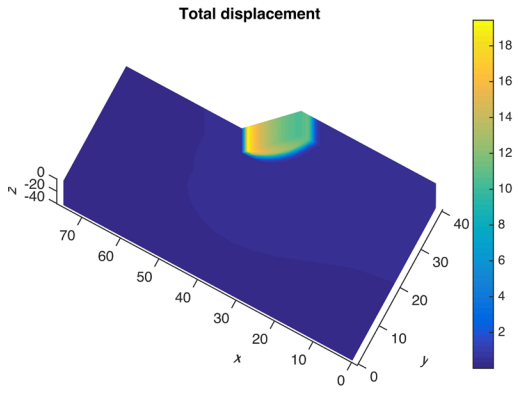

Figure 3: Total displacement and original shape at the end of the loading process.

6 CONCLUSIONS

In this paper, we have briefly summarized our parallel implementation of the Mohr-Coulomb plastic criterion, which is based on the new approach introduced in [12] and the TFETI DDM. This approach allows us to compute bigger benchmarks and estimate the limit value to get closer to the expected value of 4.045 (which is the experimentally measured limit value of the slope stability experiment).

ACKNOWLEDGEMENTS

The work was also supported by The Ministry of Education, Youth and Sports from the National Programme of Sustainability (NPU II) project "IT4Innovations excellence in science - LQ1602" and from the Large Infrastructures for Research, Experimental Development and Innovations project "IT4Innovations National Supercomputing Center LM2015070"; by the internal student grant competition project SP2017/169 "PERMON toolbox development III". The authors acknowledge the Czech Science Foundation (GACR) project no. 15-18274S.

REFERENCES

[1] M. Cermak, V. Hapla, J. Kruzik, A. Markopoulos, and A. Vasatova. Comparison of different FETI preconditioners for elastoplasticity. *Computers & Mathematics with Applications*, forthcoming.

[2] M. Cermak and S. Sysala. How to simplify return-mapping algorithms in computational plasticity: Part 1-main idea. In *Proceedings of the 8th International Conference on Computational Plasticity - Fundamentals and Applications, COMPLAS 2015*, pages 843–854, 2015.

[3] M. Cermak and S. Sysala. How to simplify return-mapping algorithms in computational plasticity: Part 2 - implementation details and experiments. In *Proceedings of the 8th International Conference on Computational Plasticity - Fundamentals and Applications, COMPLAS 2015*, 2015.

[4] E. A. de Souza Neto, D. Peri, and D. R. J. Owen. *Computational Methods for Plasticity*. Wiley-Blackwell, oct 2008.

[5] Z. Dostál, D. Horák, and R. Kučera. Total FETI – an easier implementable variant of the FETI method for numerical solution of elliptic PDE. *Communications in Numerical Methods in Engineering*, 22(12):1155–1162, 2006.

[6] C. Farhat, J. Mandel, and F.-X. Roux. Optimal convergence properties of the FETI domain decomposition method. *Computer Methods in Applied Mechanics and Engineering*, 115:365–385, 1994.

[7] C. Farhat and F.-X. Roux. A method of finite element tearing and interconnecting and its parallel solution algorithm. *International Journal for Numerical Methods in Engineering*, 32(6):1205–1227, 1991.

[8] Y. Fragakis and M. Papadrakakis. The mosaic of high performance domain decomposition methods for structural mechanics: formulation, interrelation and numerical efficiency of primal and dual methods. *Computer Methods in Applied Mechanics and Engineering*, 192(35-36):3799–3830, 2003.

[9] V. Hapla et al. PERMON (Parallel, Efficient, Robust, Modular, Object-oriented, Numerical) web pages, 2015.

[10] G. Karypis and V. Kumar. A fast and high quality multilevel scheme for partitioning irregular graphs. *SIAM Journal on Scientific Computing*, 20(1):359–392, 1998.

[11] L. Qi and J. Sun. A nonsmooth version of newton's method. *Mathematical Programming*, 58(1-3):353–367, jan 1993.

[12] S. Sysala and M. Cermak. Subdifferential-based implicit return-mapping operators in mohr-coulomb plasticity. *ZAMM Zeitschrift fur Angewandte Mathematik und Mechanik*, forthcoming.

[13] M. Čermák, V. Hapla, D. Horák, M. Merta, and A. Markopoulos. Total-FETI domain decomposition method for solution of elasto-plastic problems. *Advances in Engineering Software*, 84(0):48–54, 2015.

[14] M. Čermák, T. Kozubek, S. Sysala, and J. Valdman. A TFETI domain decomposition solver for elastoplastic problems. *Applied Math. and Comp*, 231:634–653, 2014.